EARTHQUAKE ENGINEERING AND STRUCTURAL DYNAMICS
Earthquake Engng Struct. Dyn. 2005; **00**:1–22 *Prepared using* eqeauth.cls *[Version: 2002/11/11 v1.00]*

Developing efficient scalar and vector intensity measures for IDA capacity estimation by incorporating elastic spectral shape information‡

Dimitrios Vamvatsikos[1,*,†] and C. Allin Cornell[2]

[1] *Department of Civil Engineering, National Technical University of Athens, Greece*
[2] *Department of Civil and Environmental Engineering, Stanford University, CA 94305-4020, U.S.A.*

SUMMARY

Scalar and vector Intensity Measures are developed for the efficient estimation of limit-state capacities through Incremental Dynamic Analysis (IDA) by exploiting the elastic spectral shape of individual records. IDA is a powerful analysis method that involves subjecting a structural model to several ground motion records, each scaled to multiple levels of intensity (measured by the Intensity Measure or *IM*), thus producing curves of structural response parameterized by the *IM* on top of which limit-states can be defined and corresponding capacities can be calculated. When traditional *IM*s are used, such as the peak ground acceleration or the first-mode spectral acceleration, the *IM*-values of the capacities can display large record-to-record variability, forcing the use of many records to achieve reliable results. By using single optimal spectral values as well as vectors and scalar combinations of them on three multistory buildings significant dispersion reductions are realized. Furthermore, IDA is extended to vector *IM*s, resulting in intricate fractile IDA surfaces. The results reveal the most influential spectral regions/periods for each limit-state and building, illustrating the evolution of such periods as the seismic intensity and the structural response increase towards global collapse. The ordinates of the elastic spectrum and the spectral shape of each individual record are found to significantly influence the seismic performance and they are shown to provide promising candidates for highly efficient *IM*s. Copyright © 2005 John Wiley & Sons, Ltd.

KEY WORDS: performance-based earthquake engineering; incremental dynamic analysis; capacity; intensity measure; limit-state; nonlinear

1. INTRODUCTION

An important aspect of Performance-Based Earthquake Engineering (PBEE) is calculating, for a given building, capacities for the limit-states of interest and their corresponding mean annual frequencies of exceedance. A promising method that has been developed to meet these needs is Incremental Dynamic Analysis (IDA). It involves performing nonlinear dynamic analyses of the structural model under a

*Correspondence to: Dimitrios Vamvatsikos, Theagenous 11, Athens 11634, Greece.
†E-mail: divamva@stanfordalumni.org
‡Based on a short paper presented at the 13th World Conference on Earthquake Engineering, Vancouver, 2004

Contract/grant sponsor: Sponsors of the Reliability of Marine Structures Affiliates Program of Stanford University

Received ? May 2004
Revised 9 March 2005
Accepted 11 March 2005

suite of ground motion records, each scaled to several intensity levels designed to force the structure all the way from elasticity to final global dynamic instability (Vamvatsikos and Cornell [1]). Thus, we can generate IDA curves of the structural response, as measured by an Engineering Demand Parameter (*EDP*, e.g., the maximum peak interstory drift ratio $\theta_{\max}$), versus the ground motion intensity level, measured by an Intensity Measure (*IM*, e.g., peak ground acceleration, PGA, or the 5%-damped first-mode spectral acceleration $S_a(T_1,5\%)$). Subsequently, limit-states (e.g., Immediate Occupancy or Collapse Prevention in FEMA [2]) can be defined on each IDA curve and the corresponding capacities can be calculated. The resulting capacities are then summarized, for example into appropriate fractiles, combined with probabilistic seismic hazard analysis results and integrated within a suitable PBEE framework to allow the calculation of the mean annual frequencies of exceeding each limit-state (Vamvatsikos and Cornell [3]).

It is an unavoidable fact that the IDA curves and, correspondingly, the limit-state capacities display large record-to-record variability even for the simplest of structures, e.g., oscillators (Vamvatsikos and Cornell [4]). This observed dispersion is closely connected to the *IM* used; some *IM*s are more *efficient* than others, better capturing and explaining the differences from record to record, thus bringing the results from all records closer together. Compare, for example, Figures 1(a) and 1(b) where thirty IDA curves for a 9-story steel moment-resisting frame are plotted using PGA and $S_a(T_1,5\%)$, respectively, as the *IM*. In both cases the variability from record to record is indeed remarkable, especially considering that the thirty records were chosen to represent a scenario earthquake and belong to a narrow magnitude and distance bin (Table I). However, PGA (Figure 1(a)) is proven to be deficient relative to $S_a(T_1,5\%)$ (Figure 1(b)) in expressing the limit-state capacities of the 9-story; it increases the variability between the curves and, correspondingly, the dispersion of capacities everywhere on the IDAs. On the other hand, even the improvement achieved by $S_a(T_1,5\%)$ still leaves something to be desired, as dispersions remain in the order of 40% – 50%.

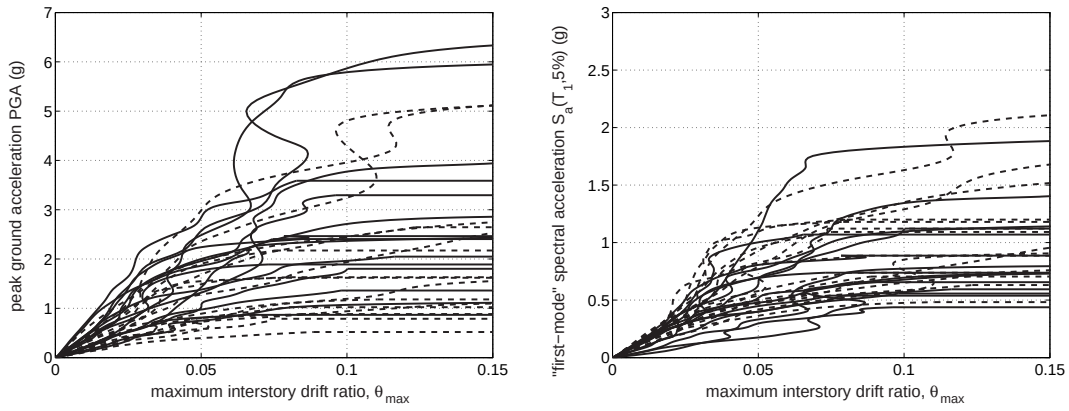

(a) Thirty IDA curves versus PGA

(b) Thirty IDA curves versus $S_a(T_1,5\%)$

Figure 1. IDA curves for a $T_1 = 2.4$ sec, 9-story steel moment-resisting frame with fracturing connections plotted against (a) PGA and (b) $S_a(T_1,5\%)$.

Why should we search for such a better *IM*? There is a clear computational advantage if we can select it *a priori*, before the IDA is performed. By reducing the variability in the IDA curves we need fewer records to achieve a given level of confidence in estimating the fractile *IM*-values of limit-state

capacities and the mean annual frequencies of limit-state exceedance. Typically, a reduction of the *IM*-capacity dispersion by a factor of two means that we need four times fewer records to gain the same confidence in the fractile *IM*-capacity results (e.g., Vamvatsikos and Cornell [3]): We could get same quality results by using about eight instead of thirty records. Obviously, the computational savings would be enormous.

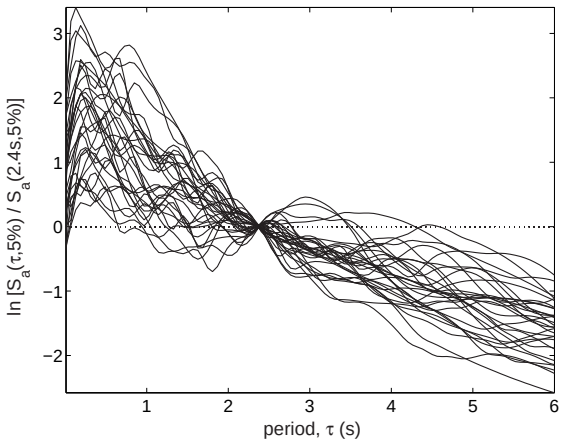

Figure 2. The 5%-damped elastic acceleration spectra for thirty scenario records, normalized to the first-mode period of the 9-story building.

Additionally, it is speculated that increasing the efficiency of the *IM* may also lead to improved *sufficiency* as well. A sufficient *IM* produces the same distribution of demands and capacities independently of the record selection, e.g., there is no bias in the fractile *IM*-capacities if we select records with low rather than high magnitudes or if the records do or do not contain directivity pulses (Luco [5]). The goals of efficiency and sufficiency are not necessarily tied together as the former aims at reducing the variability in the IDA results while the latter at reducing (or eliminating) their dependance on record characteristics other than the *IM*. Still, using a more efficient *IM* will bring the results from all records closer, and similarly bring close the IDA curves of records coming from different magnitudes or containing different directivity pulses, thus reducing the importance of any magnitude or directivity dependance.

While $S_a(T_1,5\%)$ is found to be both efficient and sufficient for first-mode-dominated, moderate period structures when directivity is not present (Shome and Cornell [6]), it is not necessarily so for other cases (Luco [5]). Therefore, it is important to try and improve our *IM*s beyond the capabilities of $S_a(T_1,5\%)$. Figure 2 may provide some clues; therein we have plotted the 5%-damped acceleration spectra of the thirty records chosen to represent a scenario earthquake and appearing in Table I. The spectra have been normalized by $S_a(2.4\text{s},5\%)$, i.e., the value of $S_a(T_1,5\%)$ at the first-mode period $T_1 = 2.4$s of the 9-story building that we are using as an example. There is obviously much variability in the individual spectra that cannot be captured by just $S_a(T_1,5\%)$. A structure is not always dominated by a single frequency and even then, when the structure sustains damage its properties change. Thus, spectral regions away from the elastic first-mode period, T_1, may become more influential. By taking the differences in the individual spectral shapes into account, we may be able to reduce the variability in the IDA curves and come up with an overall better *IM*.

Such information may be incorporated into the *IM* by using appropriate inelastic spectral values

Table I. The suite of thirty ground motion records used.

No	Event	Station	ϕ° *	Soil†	M‡	R§ (km)	PGA (g)
1	Loma Prieta, 1989	Agnews State Hospital	090	C,D	6.9	28.2	0.159
2	Northridge, 1994	LA, Baldwin Hills	090	B,B	6.7	31.3	0.239
3	Imperial Valley, 1979	Compuertas	285	C,D	6.5	32.6	0.147
4	Imperial Valley, 1979	Plaster City	135	C,D	6.5	31.7	0.057
5	Loma Prieta, 1989	Hollister Diff. Array	255	–,D	6.9	25.8	0.279
6	San Fernando, 1971	LA, Hollywood Stor. Lot	180	C,D	6.6	21.2	0.174
7	Loma Prieta, 1989	Anderson Dam Downstrm	270	B,D	6.9	21.4	0.244
8	Loma Prieta, 1989	Coyote Lake Dam Downstrm	285	B,D	6.9	22.3	0.179
9	Imperial Valley, 1979	El Centro Array #12	140	C,D	6.5	18.2	0.143
10	Imperial Valley, 1979	Cucapah	085	C,D	6.5	23.6	0.309
11	Northridge, 1994	LA, Hollywood Storage FF	360	C,D	6.7	25.5	0.358
12	Loma Prieta, 1989	Sunnyvale Colton Ave	270	C,D	6.9	28.8	0.207
13	Loma Prieta, 1989	Anderson Dam Downstrm	360	B,D	6.9	21.4	0.24
14	Imperial Valley, 1979	Chihuahua	012	C,D	6.5	28.7	0.27
15	Imperial Valley, 1979	El Centro Array #13	140	C,D	6.5	21.9	0.117
16	Imperial Valley, 1979	Westmoreland Fire Station	090	C,D	6.5	15.1	0.074
17	Loma Prieta, 1989	Hollister South & Pine	000	–,D	6.9	28.8	0.371
18	Loma Prieta, 1989	Sunnyvale Colton Ave	360	C,D	6.9	28.8	0.209
19	Superstition Hills, 1987	Wildlife Liquefaction Array	090	C,D	6.7	24.4	0.18
20	Imperial Valley, 1979	Chihuahua	282	C,D	6.5	28.7	0.254
21	Imperial Valley, 1979	El Centro Array #13	230	C,D	6.5	21.9	0.139
22	Imperial Valley, 1979	Westmoreland Fire Station	180	C,D	6.5	15.1	0.11
23	Loma Prieta, 1989	Halls Valley	090	C,C	6.9	31.6	0.103
24	Loma Prieta, 1989	WAHO	000	-,D	6.9	16.9	0.37
25	Superstition Hills, 1987	Wildlife Liquefaction Array	360	C,D	6.7	24.4	0.2
26	Imperial Valley, 1979	Compuertas	015	C,D	6.5	32.6	0.186
27	Imperial Valley, 1979	Plaster City	045	C,D	6.5	31.7	0.042
28	Loma Prieta, 1989	Hollister Diff. Array	165	–,D	6.9	25.8	0.269
29	San Fernando, 1971	LA, Hollywood Stor. Lot	090	C,D	6.6	21.2	0.21
30	Loma Prieta, 1989	WAHO	090	–,D	6.9	16.9	0.638

* Component † USGS, Geomatrix soil class ‡ moment magnitude §closest distance to fault rupture

(Luco [5]). This seems to be a promising method, as it directly incorporates the influence of the record on an oscillator that can yield and experience damage in a way similar to the structure. Still, in the context of PBEE, the use of inelastic spectral values requires new, custom-made attenuation relationships. On the other hand, using the elastic spectral values allows the use of the attenuation laws available in the literature. Therefore, there is still much to be gained from the use of *IM*s based on elastic spectra.

Actually, studies by Shome and Cornell [6], Carballo and Cornell [7], Mehanny and Deierlein [8] and Cordova *et al.* [9] have shown that the elastic spectral shape can be a useful tool in determining an improved *IM*. Shome and Cornell [6] found that the inclusion of spectral values at the second-mode period (T_2) and at the third-mode (T_3), namely $S_a(T_2,5\%)$ and $S_a(T_3,5\%)$, significantly improved the efficiency of $S_a(T_1,5\%)$ for tall buildings. Carballo and Cornell [7] observed greatly reduced variability in the *EDP* demands when spectral shape information was included by compatibilizing a suite of records to their median elastic spectrum. In addition, Mehanny and Deierlein [8] and Cordova *et al.* [9] observed an improvement in the efficiency of $S_a(T_1,5\%)$ when an extra period, longer than

the first-mode was included by employing an *IM* of the form $S_a(T_1,5\%)^{1-\beta}\, S_a(c\cdot T_1,5\%)^{\beta}$ (with suggested values $\beta = 0.5$, $c = 2$). They also presented some evidence suggesting that sufficiency may be improved as well, since the new *IM* made the IDA curves of several near-fault records practically indistinguishable, regardless of the directivity-pulse period. Motivated by such encouraging results we are going to use the methodology and tools developed by Vamvatsikos and Cornell [1, 3] to better investigate the potential of incorporating elastic spectral shape information in *IM*s to reduce the dispersion in IDA results.

2. METHODOLOGY

We will employ three different structures for our investigation into the potential use of the elastic acceleration spectrum. These will be a $T_1 = 1.8$s 5-story steel chevron-braced frame and two steel moment-resisting frames designed for Los Angeles: a $T_1 = 2.4$s 9-story with fracturing connections and a $T_1 = 4$s 20-story with ductile connections. In all cases we used two-dimensional centerline models. The 5-story model includes ductile members and connections but realistically buckling braces (Bazzurro and Cornell [10]). The 9-story model incorporates ductile members, shear panels and realistically fracturing reduced beam section connections, while it includes the influence of interior gravity frames (Lee and Foutch [11]). The 20-story model (Luco and Cornell [12]) has ductile members and connections and it also accounts for the influence of the interior gravity frames. Finally, all models include a first-order treatment of global geometric nonlinearities (P-Δ effects).

To perform IDA we used the suite of thirty records representing a scenario earthquake that was introduced earlier in Table I. These belong to a bin of relatively large magnitudes of 6.5 – 6.9 and moderate distances, all recorded on firm soil and bearing no marks of directivity. Each of these records was appropriately scaled to cover the entire range of structural response for each building, from elasticity, to yielding, and finally global dynamic instability. At each scaling level a nonlinear dynamic analysis was performed and a single scalar was used to describe the structural response, the Engineering Demand Parameter *EDP* according to current Pacific Earthquake Engineering Research (PEER) Center terminology (previously known as the Damage Measure *DM*, e.g., Vamvatsikos and Cornell [1]) . This will be $\theta_{\max}$ in our case. The scaling level and the associated ground motion intensity can be expressed by the selected *IM*, which will initially be $S_a(T_1,5\%)$ for our investigation. By interpolating such pairs of $S_a(T_1,5\%)$ and $\theta_{\max}$ values for each individual record we get thirty continuous IDA curves for each of the three buildings, shown as an example in Figure 1(b) for the 9-story.

While usually only a handful of distinct limit-states of practical value would be defined on the IDA curves (e.g., Immediate Occupancy or Collapse Prevention in FEMA [2]), we will proceed to define a continuum of limit-states that completely cover the structural response: Each will be defined at a given $\theta_{\max}$ value to represent the capacity of the structure at a specific damaged state and level of response. Finally, the appropriate $S_a^c(T_1,5\%)$-values will be calculated, i.e., the values of $S_a(T_1,5\%)$-capacity for each record and each limit-state or value of $\theta_{\max}$ (Vamvatsikos and Cornell [1]). Our ultimate goal is to minimize the dispersion in the *IM*-values of capacities for each limit-state *individually* by selecting appropriate spectral values or vectors and functions of spectral values to be the *IM*. As a measure of the dispersion we will use the standard deviation of the logarithm of the *IM*-capacities, which is a natural choice for values that are approximately lognormally distributed (e.g., Shome and Cornell [6]).

Fortunately, no further dynamic analyses are needed to change from $S_a(T_1,5\%)$ to other *IM*s and perform this dispersion-minimization; all we need to do is to transform each limit-state's $S_a^c(T_1,5\%)$-values in the coordinates of the trial *IM*s and calculate their new dispersion. For example, if we want

the dispersion of the capacities in PGA terms, then for each unscaled record (or at a scale factor of one) we know both the PGA and $S_a(T_1,5\%)$-values and the former can be appropriately scaled by the same factor that the value of $S_a^c(T_1,5\%)$ implies; e.g., for the 9-story building, the unscaled record #5 (Table I) has $S_a(T_1,5\%) = 0.114$g and PGA $= 0.279$g, while global instability occurs at $S_a^c(T_1,5\%) = 0.49$g, representing a scale factor of $0.49/0.114 \approx 4.3$. Hence, the *IM*-capacity at the global instability limit-state in PGA terms is $\text{PGA}^c = 4.3 \cdot 0.279 = 1.20$g. Similarly we can accomplish such transformations for any *IM* based on elastic spectral values. Thus, we are taking full advantage of the observations in Vamvatsikos and Cornell [3], by appropriately postprocessing the existing dynamic runs instead of performing new ones.

The adopted approach in evaluating the candidate *IM*s is very different from the one used by Shome and Cornell [6], Mehanny and Deierlein [8], Cordova *et al.* [9] and Luco [5]. There, the focus is on demands, i.e., *EDP*-values, all four studies looking for a single "broad-range" *IM* that will improve efficiency for all damage levels of a given structure. On the other hand, our search will be more focused, zeroing on each limit-state separately to develop a "narrow-range" *IM* that will better explain the given limit-state rather than all of them. Thus, we are able to follow the evolution of such *IM*s as damage increases in the structure, hopefully gaining valuable intuition in the process. Still, since we use only $\theta_{\max}$ to define the structural limit-states, our observations may or may not be applicable when limit-states are defined on other structural response measures (e.g., peak floor accelerations).

The initial focus of our investigation will be on the efficiency gained by incorporating elastic spectrum information in the *IM*. We will start by investigating single spectral coordinates. This does not constitute an investigation of spectral *shape* per se as it focuses on the use of just one value at one period. Still, it will provide a useful basis as we expand our trial *IM*s to include vectors and scalar combinations of several spectral values. Another important issue will be the robustness offered by each *IM*, i.e., how much efficiency it retains when the user selects spectral values other than those chosen by the dispersion-minimization process. This is a key question when trying to identify *a priori* an appropriate *IM* in order to take advantage of its efficiency and use fewer records in the analysis. We are not aiming to provide the final answer for the best *a priori IM*, but rather to investigate the efficiency and the potential for practical implementation offered by several promising candidates.

3. USING A SINGLE SPECTRAL VALUE

The use of a single spectral value, usually at the first-mode of the structure, i.e., $S_a(T_1,5\%)$, has seen widespread use for IDAs, having being incorporated into the FEMA [2] guidelines and used throughout most of the current research. Obviously, it is an accurate measure for SDOF systems or first-mode-dominated structures in the elastic range. However, when higher modes are important or the structure deforms into the nonlinear range, it may not be optimal. There seems to be a consensus that when structures are damaged and move into the nonlinear region, period lengthening will occur (e.g., Cordova *et al.* [9]). In that sense, there may be some merit in looking for elastic spectral values at longer or, in general, different periods than the first-mode. Therefore we will conduct a search across all periods in the spectrum to determine the one that most reduces the variability in the *IM*-values of limit-state capacities.

Some representative results are shown in Figure 3 for the 5-story building, for limit-states at four levels of $\theta_{\max}$ (Figure 4), namely 0.01% (elastic), 0.7% (early inelastic), 1% (highly nonlinear) and $+\infty$ (global instability). The structure has obviously insignificant higher modes, since $S_a(T_1,5\%)$ produces practically zero dispersion for the capacities in the elastic region (Figure 3, (a)-line). As the

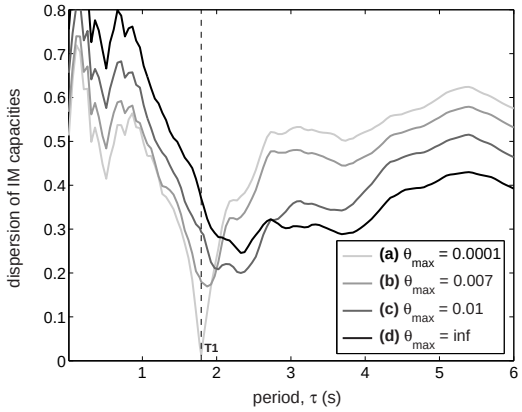

Figure 3. Dispersion of the $S_a^c(\tau,5\%)$-values versus period τ for four limit-states for the 5-story building.

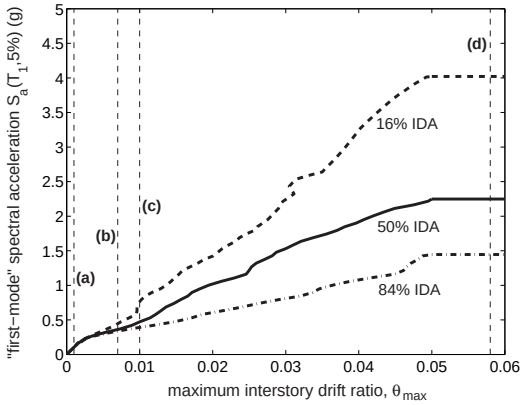

Figure 4. The fractile IDA curves and capacities for four limit-states (Figure 3) of the 5-story building.

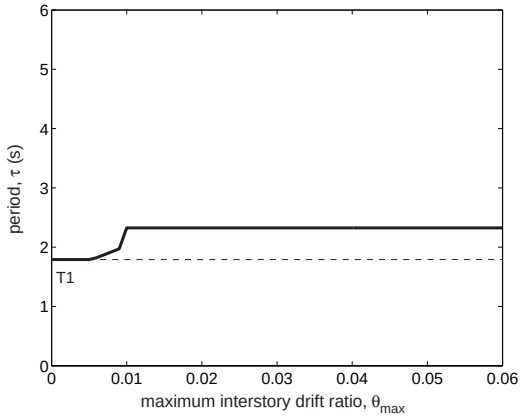

Figure 5. The optimal period τ as it evolves with $\theta_{\max}$ for the 5-story building.

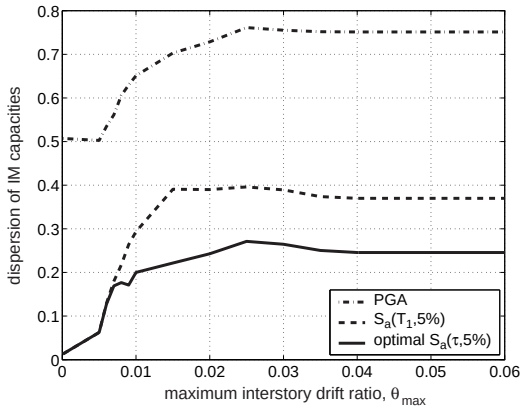

Figure 6. The dispersion for the optimal $S_a(\tau,5\%)$ compared to $S_a(T_1,5\%)$ and PGA, versus the limit-state definition, $\theta_{\max}$, for the 5-story building.

structure becomes progressively more damaged the optimal period τ moves away from T_1, lengthening to higher values as expected. Initially, only a narrow band of periods around the optimal τ display low dispersions. When close to global collapse (Figure 3, (d)-line), this band around the optimal period increases so that any period from 2s to 4s will achieve low dispersion, at worst 30% compared to about 40% when using $S_a(T_1,5\%)$. A summary of the results is shown in Figure 5, where the optimal period is shown versus the $\theta_{\max}$-value of all the limit-states considered, while the best achieved dispersion is presented in Figure 6, compared against the dispersion when using PGA and $S_a(T_1,5\%)$. As observed earlier, the optimal period increases after yielding, from $\tau = T_1$ to $\tau = 2.4$s. Similarly, the dispersion increases for all three *IM*s in Figure 6, but with the use of the optimal period the efficiency is improved at least by 40% compared to $S_a(T_1,5\%)$.

Similar results for the 9-story building are presented in Figure 7, for the limit-states appearing in Figure 8 at $\theta_{\max}$ equal to 0.5% (elastic), 5% (inelastic), 10% (close to global collapse) and $+\infty$ (global

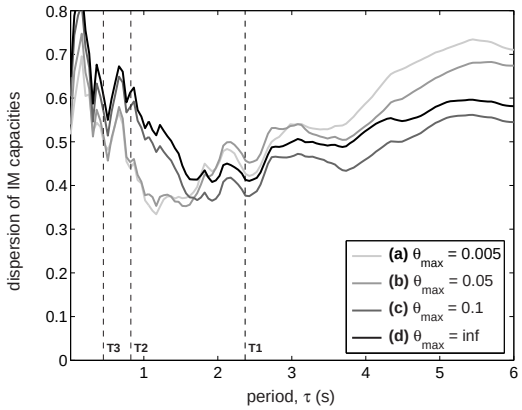

Figure 7. Dispersion of the $S_a^c(\tau,5\%)$ values versus period τ for four limit-states for the 9-story building.

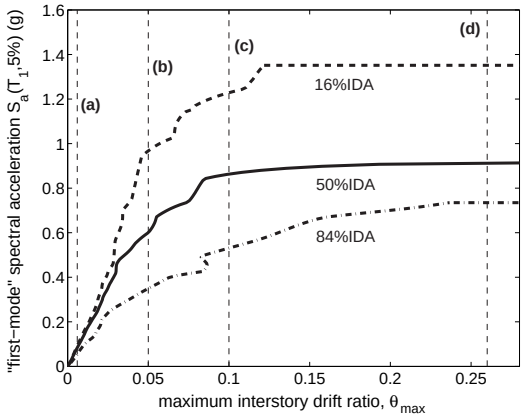

Figure 8. The fractile IDA curves and capacities for four limit-states (Figure 7) of the 9-story building.

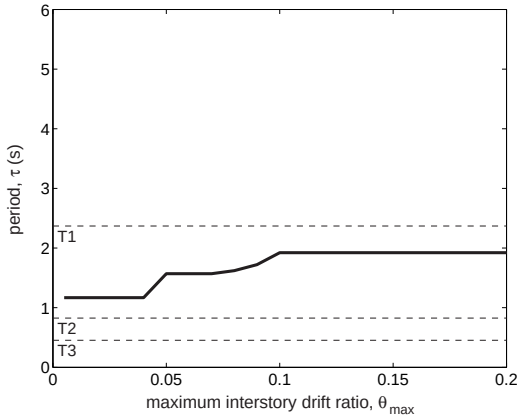

Figure 9. The optimal period τ as it evolves with $\theta_{\max}$ for the 9-story building.

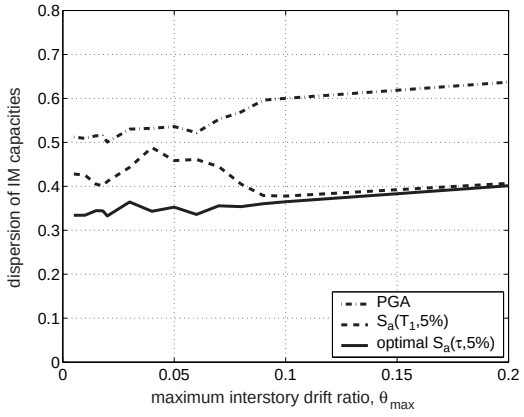

Figure 10. Dispersion for the optimal $S_a(\tau,5\%)$ compared to $S_a(T_1,5\%)$ and PGA, versus the limit-state definition, $\theta_{\max}$, for the 9-story building.

instability). The building has significant higher modes, as evident in Figure 7 [(a)-line], since the first mode is not optimal even in the elastic region. While all three modes, T_1, T_2 and T_3, seem to locally produce some dispersion reduction, the overall best single period lies somewhere between the T_1 and T_2, at $\tau \approx 1.2$s. As damage increases the optimal period lengthens to higher values, finally settling close to T_1 when global instability occurs (Figure 7, (d)-line). In Figure 9, the results are summarized for all limit-states, showing the gradual lengthening of the optimal period. Similarly, in Figure 10 the optimal dispersion thus achieved is compared versus the performance of PGA and $S_a(T_1,5\%)$. Remarkably, only in the elastic and near-elastic region does this single optimal spectral value provide some improvement over $S_a(T_1,5\%)$, in the order of 10%; close to global collapse no gains are realized.

For the 20-story structure the results for four limit-states are shown in Figure 11, for $\theta_{\max}$ equal to 0.5% (elastic), 2% (near-elastic), 10% (close to global collapse) and $+\infty$ (global instability); each limit-state is shown versus the fractile IDAs in Figure 12. This is a building where higher modes are even

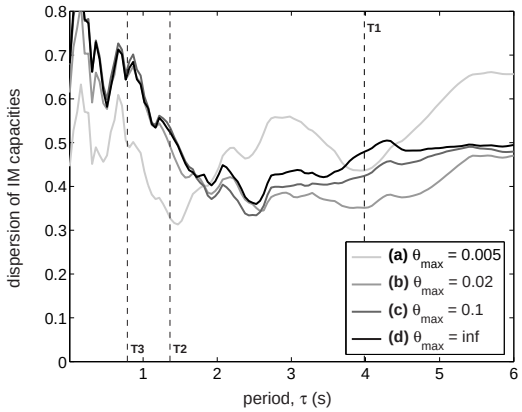

Figure 11. Dispersion of the $S_a^c(\tau,5\%)$-values versus period τ for four limit-states of the 20-story building.

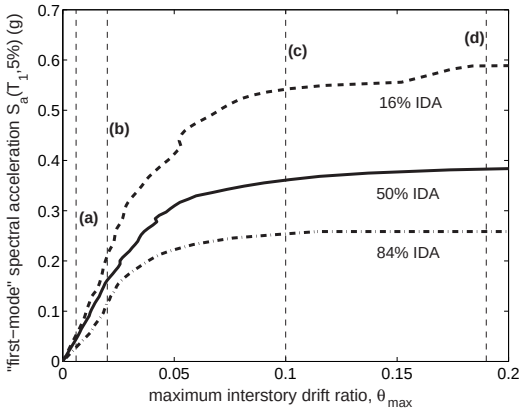

Figure 12. The fractile IDA curves and capacities for four limit-states (Figure 11) of the 20-story building.

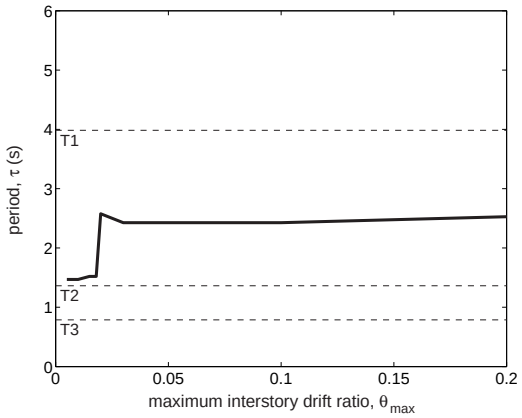

Figure 13. The optimal period τ as it evolves with $\theta_{\max}$ for the 20-story building.

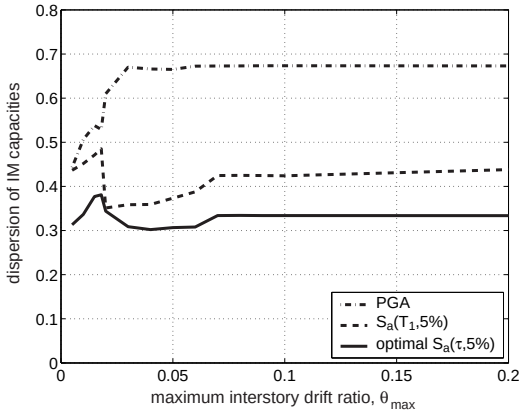

Figure 14. Dispersion for the optimal $S_a(\tau,5\%)$ compared to $S_a(T_1,5\%)$ and PGA, versus the limit-state definition, $\theta_{\max}$, for the 20-story building.

more important, and by looking at Figure 11 [(a)-line] it seems that, at least initially, the second-mode period T_2 manages to explain more than T_1 in the dispersion of the *IM* capacity values. The limit-states are defined on $\theta_{\max}$, the maximum of the story drifts, which often appears in the upper stories at low ductilities and is thus quite sensitive to the higher frequencies. As damage increases the optimal period moves away from T_2 and at global collapse reaches a value somewhere in the middle of T_1 and T_2, at $\tau \approx 2.5$s. In Figure 13 the summarized results confirm the above observations for all limit-states. Similarly to the 9-story only small reductions in dispersion are realized with the use of one spectral coordinate (Figure 14). At least, in this case, using a single optimal period seems to achieve somewhat better performance than $S_a(T_1,5\%)$ close to global collapse.

Summarizing our observations, the use of a single optimal spectral value seems to offer some benefits, but mostly to structures with insignificant higher modes. For such structures it seems relatively easy to identify the optimal period, as it is invariably an appropriately lengthened value of the first-

mode period T_1. One could almost say that practically any (reasonably) lengthened first-mode period will work well. On the other hand, when higher modes are present, one spectral value is probably not enough. There do exist specific periods that one can use to reduce the variability, but they appear in a very narrow range and are difficult to pinpoint as damage increases. It would be difficult to pick *a priori* a single period for such structures as a slight miss will probably penalize the dispersion considerably.

Most probably, the reason behind this apparent difficulty is that even in the nonlinear range such structures are sensitive to more than one frequency. Thus, our attempt to capture this effect with just one period results in the selection of some arbitrary spectral coordinate that happens to provide the right "mix" of spectral values at the significant frequencies. Looking at all the previous figures it becomes obvious that missing by a little bit will again, in most cases, pump up the dispersion significantly. Obviously, this one period is not a viable solution for any but the structures dominated by the first-mode. On the other hand, the introduction of another spectral value, to form a vector or an appropriate scalar combination of two periods, might prove better.

4. USING A VECTOR OF TWO SPECTRAL VALUES

The use of more than one discrete spectral value necessitates the development of a framework for the use of vector *IM*s. While the definitions set forth in Vamvatsikos and Cornell [1] do provide for a vector *IM*, up to now no formal framework has been developed on how to postprocess and summarize such IDAs. So, before we proceed with our spectral shape investigation, we will propose a methodology to deal with vector *IM*s.

4.1. Postprocessing IDAs with vector IMs

The most important thing that we must keep in mind is that the IDA per se remains unchanged and no need exists to rerun the results that we have acquired; this is all about postprocessing, as explained in Vamvatsikos and Cornell [3]. On the other hand, there are some conceptual differences between a scalar and a vector of *IM*s. Since the *IM* must in both cases represent the scaling of the ground motion record, the scalar *IM* has to be scalable, i.e., be a function of the scale factor of the record (Vamvatsikos and Cornell [1]). However, for a vector of *IM*s it would be redundant and often confusing if more than one of the elements were scalable. Hence, we will focus on vectors where only one of the elements can be scaled, while the others are scaling-independent. That is not to say, for example, that when we have $S_a(T_1,5\%)$ in a vector, other spectral values are not acceptable. Rather, we will replace such extra spectral values by their ratio over $S_a(T_1,5\%)$ (and similarly normalize any other scalable *IM*); thus, we convey only the additional information that the new elements in the vector bring in with respect to our primary scalable (scalar) *IM*. In this case it is quite precise to speak of this additional information (one or more additional spectral ratios) as reflecting the influence of spectral shape (rather than the amplitude of the record).

Following a similar procedure as for a single scalable *IM*, we will use splines to interpolate the discrete IDA runs for each record versus the scalable *IM* from the vector (Vamvatsikos and Cornell [1]). Then, we can plot the IDA curves for all records versus the elements of the vector, as in Figure 15 for the 5-story braced frame and a vector of $S_a(T_1,5\%)$ (scalable) and the spectral ratio $R_{\text{sa}}(1.5,T_1) = S_a(1.5T_1,5\%)/S_a(T_1,5\%)$ (non-scalable). Contrary to the usual practice of plotting the *IM* on the vertical axis, we will now plot both *IM*s on the two horizontal axes and put the *EDP* on the vertical one, to visually separate the "input" from the "output". As a consequence the flatlines are now

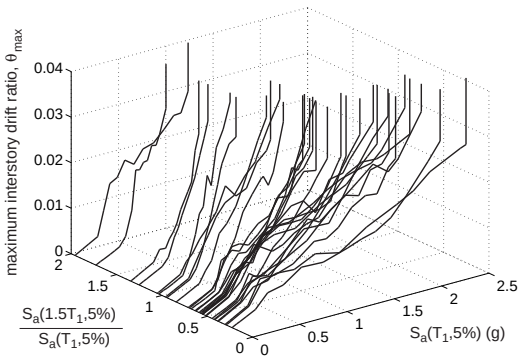

Figure 15. The thirty IDA curves for the 5-story building in $S_a(T_1, 5\%)$ and $R_{\text{sa}}(1.5, T_1)$ coordinates.

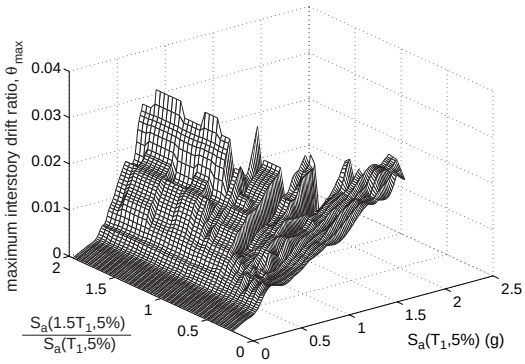

Figure 16. The median IDA surface for the 5-story building in $S_a(T_1, 5\%)$ and $R_{\text{sa}}(1.5, T_1)$ coordinates.

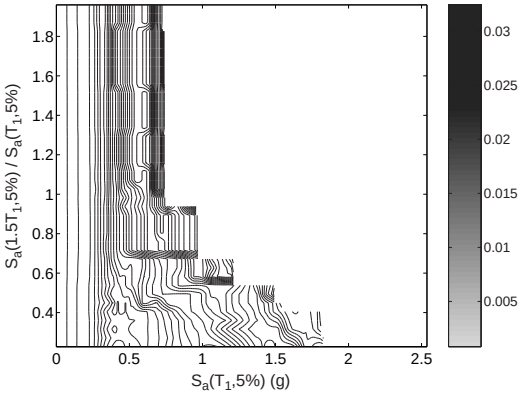

Figure 17. The median contours for thirty IDA curves for the 5-story building in $S_a(T_1, 5\%)$ and $R_{\text{sa}}(1.5, T_1)$ coordinates. Their color indicates the level of $\theta_{\max}$ as shown in the color bar.

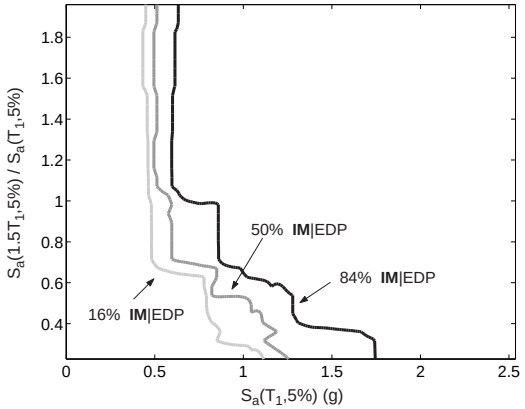

Figure 18. The 16%, 50% and 84% capacity lines at the limit-state of $\theta_{\max} = 0.016$ for the 5-story building.

vertical lines, rather than horizontal ones.

Still, we are able to interpolate only along the scalable *IM*, while for the non-scalable one we are left with separate, discrete curves. We need to take an extra step here and make the results continuous in the other *IM* as well, which is why we will introduce summarization at this point. However, we are not able to use cross-sectional fractiles, as we did for single *IM*s in Vamvatsikos and Cornell [3]. That would require several values of *EDP* at each level of the non-scalable *IM*, practically impossible with a limited number of records. We can use instead the symmetric-neighborhood running fractiles (Hastie and Tibshirani [13]) with a given window length to achieve the same purpose. The optimal window length can be chosen, e.g., through cross-validation (Efron and Tibshirani [14]), or by adopting a reasonable fraction of the sample size. In our case, we selected 30% of the sample size, i.e., used the $0.3 \times 30 = 9$ symmetrically closest records to approximate the fractile value for each level of the non-scalable *IM*. The resulting median IDA *surface* appears in Figure 16.

Now is the time to define limit-state capacities. It can be easily done using *EDP*-based rules for all limit-states, with $\theta_{\max} = +\infty$ resulting in the flatlines for global instability. Imagine horizontal planes,

each for a given *EDP*-value, cutting the IDA surface. The results can be easily visualized as contours of the fractile IDA surface, seen in Figure 17 for the median. Obviously, now the median capacity for a given limit-state is not a single point, as for scalar *IM*s, rather a whole line, as the ones appearing in Figure 17. As an example, we are showing in Figure 18 the 16%, 50% and 84% capacity lines for a limit-state at $\theta_{\max} = 1.6\%$, close to the onset of global instability. These correspond to our best estimate of the 16%, 50% and 84% vector *IM*-value of the limit-state capacity. For example, if several records had $R_{\text{sa}}(1.5,T_1) = 1.2$, then if scaled to $S_a(T_1,5\%) \approx 0.5$g (to reach the 16% capacity line) only 16% of them would cause the structure to violate the limit-state, and they would have to be scaled to only $S_a(T_1,5\%) \approx 0.6$g for 84% of them to cause limit-state exceedance. On the other hand, if another set of records were comparatively less rich in the longer periods, e.g., if $R_{\text{sa}}(1.5,T_1) = 0.5$, they would have to be scaled to $S_a(T_1,5\%) \approx 1$g to cause 50% of the records to violate this same limit-state.

In retrospect, notice that we have slightly altered the "standard" IDA post-processing, as defined by Vamvatsikos and Cornell [1, 3]. For scalar *IM*s we would first define limit-states points on each IDA and then summarize, while for vector *IM*s it is advantageous to reverse these steps. Keep in mind though that if we are using only *EDP*-based rules for the definition of limit-states, as we do here, then we can similarly reverse these steps for the scalar *IM*. The results will be exactly the same, as explained in Vamvatsikos and Cornell [3]: The $(100-x)$%-fractile IDA limit-state capacities for Immediate Occupancy and Global Instability (and all other *EDP*-based limit-states) reside on the x%-fractile IDAs. On the other hand, this is not the case for the FEMA-350 [2] definition of the Collapse Prevention limit-state. It is partially based on the change of the slope of the IDA (Vamvatsikos and Cornell [1]), therefore it is clearly not a simple *EDP*-based limit-state.

As a final note, it is important to observe how we were forced to introduce summarization over windows rather than stripes. By introducing an extra *IM*, we may have explained some of the variability in the capacities but we have also increased the dimensionality of the sample space, thus the data is more sparse. Where we used to have 30 points for each level (stripe) of the scalable *IM*, we now have only a few points for whole regions of the unscalable *IM*. Obviously, we cannot keep introducing extra dimensions, otherwise we will be facing extreme lack-of-data problems.

4.2. Investigating the vector of two spectral values

Clearly, for the 5-story building with negligible higher modes, using a vector instead of a scalar *IM* produces very impressive results. The introduction of $R_{\text{sa}}(1.5,T_1)$ provides significant insight into the seismic behavior of the 5-story, as seen in Figure 17; for records with $R_{\text{sa}}(1.5,T_1) > 1$, as its period lengthens the damaged structure falls in a more aggressive part of the spectrum and is forced to fail at earlier $S_a(T_1,5\%)$ levels, exhibiting IDAs with rapid softening. On the other hand, if $R_{\text{sa}}(1.5,T_1) < 1$ the period lengthening helps to relieve the structure allowing the IDA to harden and reach higher flatlines in terms of $S_a(T_1,5\%)$. Actually, the less aggressive the record is at longer periods (lower $R_{\text{sa}}(1.5,T_1)$) the more the IDA hardens. The introduction of the extra *IM* has helped explain some of the record-to-record variability in the $S_a(T_1,5\%)$ capacities for almost any level of *EDP*, i.e., for any limit-state.

Additional studies show that such results are not very sensitive to the spectral ratio that we choose to use. At least for the 5-story building almost any such lengthened period will provide some explanation of the variability in capacity. On the other hand though, it may not be so for other buildings. As shown for the 9-story and 20-story buildings in Figures 19 and 20 respectively, using a vector of $S_a(T_1,5\%)$ and $R_{\text{sa}}(1.5,T_1)$ yields little or no additional information compared to just $S_a(T_1,5\%)$. These buildings have significant higher-mode influence, hence we have to use a spectral coordinate at a period *lower*

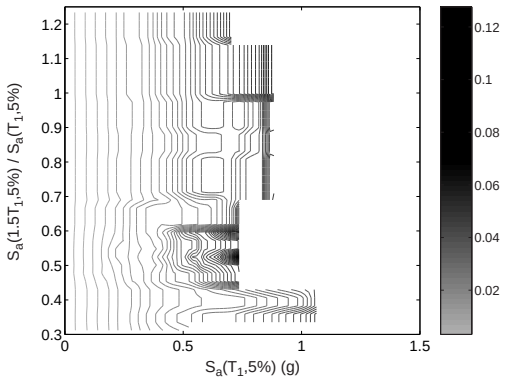

Figure 19. Median contours colored by $\theta_{\max}$ for the 9-story building in $S_a(T_1, 5\%)$ and $R_{\text{sa}}(1.5, T_1)$ coordinates. We see little improvement over $S_a(T_1, 5\%)$.

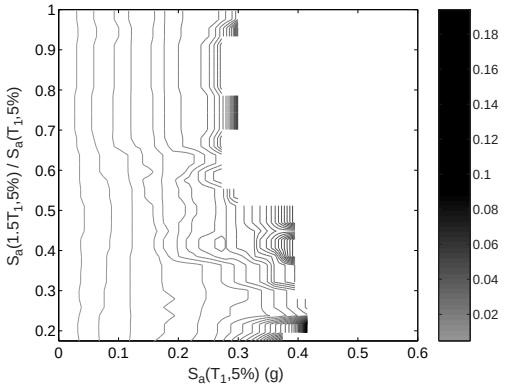

Figure 20. Median contours colored by $\theta_{\max}$ for the 20-story building in $S_a(T_1, 5\%)$ and $R_{\text{sa}}(1.5, T_1)$ coordinates. The use of a vector has small influence.

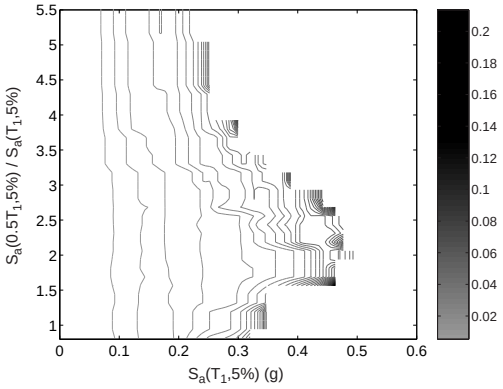

Figure 21. Median contours colored by $\theta_{\max}$ for the 20-story building in $S_a(T_1, 5\%)$ and $R_{\text{sa}}(0.5, T_1)$ coordinates. Some variability is explained but the contours are not simple.

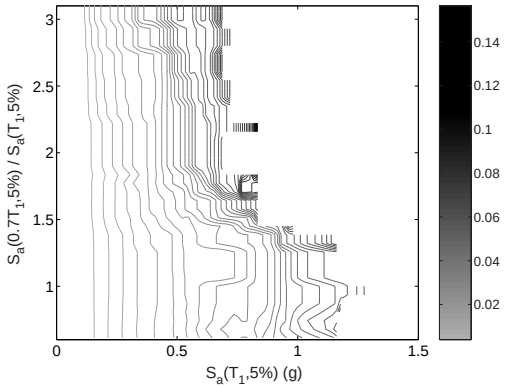

Figure 22. Median contours colored by $\theta_{\max}$ for the 9-story building in $S_a(T_1, 5\%)$ and $R_{\text{sa}}(0.7, T_1)$ coordinates. The contours have power-law shape.

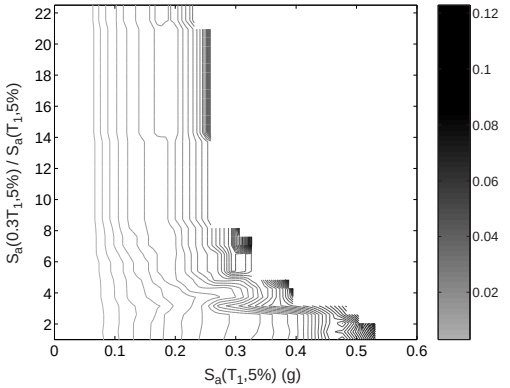

Figure 23. Median contours colored by $\theta_{\max}$ for the 20-story building in $S_a(T_1, 5\%)$ and $R_{\text{sa}}(0.3, T_1)$ coordinates. The contours have power-law shape.

than T_1 to gain resolution. Still the shape of the contours may no longer be the simple, monotonic, almost power-law shape that was observed for the 5-story. This happens, for example, in Figure 21 for the 20-story when $R_{\text{sa}}(0.5,T_1)$ is used in addition to $S_a(T_1,5\%)$ (where $0.5T_1 \approx 1.5T_2$ for this building): the most aggressive records are the ones with $R_{\text{sa}}(0.5,T_1) \approx 2$, while lower or higher values of the spectral ratio will both indicate more benign records. Still, even for these complex buildings, there exist periods that explain well the variability and even show the familiar, power-law shape of the contours, as shown for the 9-story when we use $R_{\text{sa}}(0.7,T_1)$ (where $0.7T_1 \approx 2T_2$ for the 9-story) in Figure 22, and even the 20-story when we introduce $R_{\text{sa}}(0.3,T_1)$ in Figure 23 (where $0.3T_1 \approx T_2$ for the 20-story). Clearly, there is great potential in using a vector of two spectral values, but the question remains whether the appropriate periods for its use are easy to determine, especially *a priori*.

5. USING A POWER-LAW FORM WITH TWO OR THREE SPECTRAL VALUES

By observing the power-law shape of the contours in Figures 17, 22 and 23 it becomes obvious that they can be approximated for each of the three buildings by the equation

$$S_a^c(T_1,5\%) \approx \alpha R_{\text{sa}}(1.5,T_1)^{-\beta} \tag{1}$$

where α, β are the fitted coefficients. Even though for a given building the β-value is not constant for all limit-states, as the contours have higher curvature for higher *EDP*-values, we can still specify some reasonable β-value that will be adequate for most of them. In that case, we can rewrite Equation (1) as

$$\alpha \approx S_a^c(T_1,5\%)\, R_{\text{sa}}(1.5,T_1)^{\beta} \tag{2}$$

and interpret it as follows: by multiplying $S_a^c(T_1,5\%)$ capacity values by $R_{\text{sa}}(1.5,T_1)^{\beta}$, we can bring them closer, almost to an (arbitrary) constant. In other words, $S_a(T_1,5\%)R_{\text{sa}}(1.5,T_1)^{\beta}$ is a scalar *IM* that will retain much of the vector *IM*'s ability to reduce dispersion in limit-state capacities. How much reduction it will achieve will depend on our ability to select a proper β-value and the goodness-of-fit of Equation (1) to the contour.

Not surprisingly, it is such a form that Shome and Cornell [6], Mehanny and Deierlein [8] and Cordova *et al.* [9] have used to create a new, more effective scalar *IM*. While the idea there was mostly driven by the need to be able to use existing attenuation laws to create hazard curves for the new *IM* (Cordova *et al.* [9]), they have come very close to an accurate approximation of the contour shape.

Motivated by the above results we intend to perform a search for the optimally efficient *IM* of the form

$$\begin{aligned} IM &\equiv S_a(\tau_a,5\%)^{1-\beta}\, S_a(\tau_b,5\%)^{\beta} \\ &= S_a(\tau_a,5\%)\left[\frac{S_a(\tau_b,5\%)}{S_a(\tau_a,5\%)}\right]^{\beta} \end{aligned} \tag{3}$$

where τ_a and τ_b are arbitrary periods and $\beta \in [0,1]$. Notice the difference with Shome and Cornell [6] who constrain both periods to be T_1 and T_2 respectively, or Mehanny and Deierlein [8] and Cordova *et al.* [9], who chose to constrain one of the periods to be T_1. Instead, we intend to let the optimization find the best values, τ_a, τ_b and β.

Additionally, we will investigate a power-law form containing three spectral values or, equivalently,

a single spectral value and two spectral ratios:

$$IM \equiv S_a(\tau_a,5\%)^{1-\beta-\gamma}\, S_a(\tau_b,5\%)^{\beta}\, S_a(\tau_c,5\%)^{\gamma}$$
$$= S_a(\tau_a,5\%)\left[\frac{S_a(\tau_b,5\%)}{S_a(\tau_a,5\%)}\right]^{\beta}\left[\frac{S_a(\tau_c,5\%)}{S_a(\tau_a,5\%)}\right]^{\gamma} \quad (4)$$

where τ_a, τ_b and τ_c are arbitrary periods, $\beta,\gamma \in [0,1]$ and $\beta+\gamma \leq 1$.

The optimal two periods for the 5-story building appear in Figure 24 over a range of limit-states from elasticity to global collapse. At elasticity, the two periods converge to the first mode, T_1, since the structure has practically no higher mode effects. As damage increases one of the periods hovers close to T_1 while the other increases and fluctuates about 50% higher. The optimal value of β is always about 0.5, favoring equal weighting of the two periods. Comparing Figures 6 and 26 it becomes obvious that the use of two spectral values reduces the capacity dispersion by a small amount relative to the use of a single optimal value. While $S_a(T_1,5\%)$ would achieve about 40% dispersion and a single optimal period would reduce this to 25%, the use of two periods only brings it down to 20%.

If we introduce a third spectral value for the 5-story through Equation 4, then we come up with the three optimal periods shown in Figure 25 for a range of limit-states. Again, in elasticity, the three periods start at T_1 and then they slowly separate. One period stays at about T_1 and the rest gradually increase. When close to global collapse the second one is 50% higher and the third 100% higher than T_1. Again, equal weighting seems to be the rule for all limit-states since the optimal values are $\beta \approx \gamma \approx 1/3$. The dispersion reduction is even less spectacular than before (Figure 26), reaching a level of just 18% at global collapse compared to the 20% of the two spectral values. Clearly, we have reached the limits of what the elastic spectral shape can do for this building. As expected, when higher modes are insignificant, one, maybe two, periods will be enough to determine an improved, near-optimal *IM*, cutting down dispersion by a factor of two relative to $S_a(T_1,5\%)$. Adding more complexity to the *IM* does not seem to help efficiency, as the system is not that complex itself.

When practically implementing such *IM*s before the dynamic analyses are performed, it is important that efficiency remains high even when not using the (unknown *a priori*) optimal periods. To investigate the sensitivity of the proposed scalar *IM*s we have simulated random user choices for the period(s) used for the single spectral value or the power-law combinations of two or three values. The user is supposed to have picked periods uniformly distributed within $\pm 20\%$ of the optimal values for each *IM* and to have selected equal weighting of spectral values in the power-law (i.e., $\beta = 1/2$ or $\beta = \gamma = 1/3$). Such simulations are repeated numerous times for each limit-state (i.e., value of $\theta_{\max}$) and the achieved suboptimal dispersions are calculated for each *IM*. In Figure 27 we are plotting the 84%-fractile of the resulting sample of suboptimal dispersions for the single period and the two power-law combinations versus the $\theta_{\max}$ definition of each limit-state; i.e., we are focusing on a worse-than-average scenario. For comparison, the dispersion when using $S_a(T_1,5\%)$ and when using the optimal three periods power-law is also shown. Obviously, the largest effect for the 5-story is in the elastic region, where not using T_1 is a very bad choice in all cases. In the nonlinear range, missing the optimal period seriously degrades the performance of a single *IM*, bringing its dispersion to about 30%, a fact also observed in Figure 3. On the other hand, the two and three period combinations perform relatively well, managing to keep a dispersion of about 25% and 20%. Again, just as when using a vector of two spectral values, the power-law form is quite stable, even more so than using a single spectral value, since relatively large changes away from the optimal periods do not influence significantly the dispersion reduction of the power-law *IM*. Practically, in the post-yield region, using the first mode plus e.g., a 50% increased period, with $\beta = 0.5$ (i.e., equal weight on both spectral values) will in general produce good results. Actually these conclusions are quite in agreement with Cordova *et al.* [9].

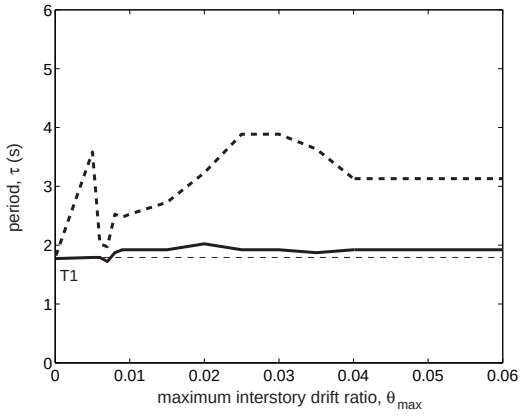

Figure 24. The two optimal periods τ_a, τ_b as they evolve with $\theta_{\max}$ for the 5-story building.

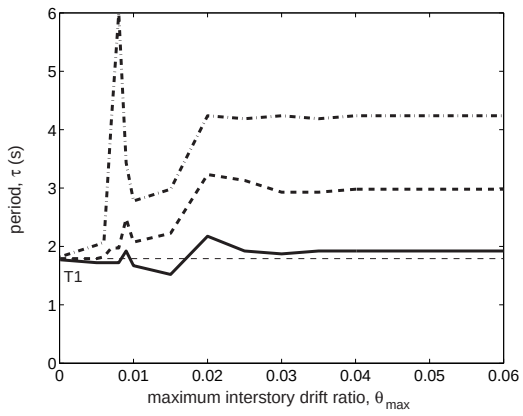

Figure 25. The three optimal periods τ_a, τ_b, τ_c as they evolve with $\theta_{\max}$ for the 5-story building.

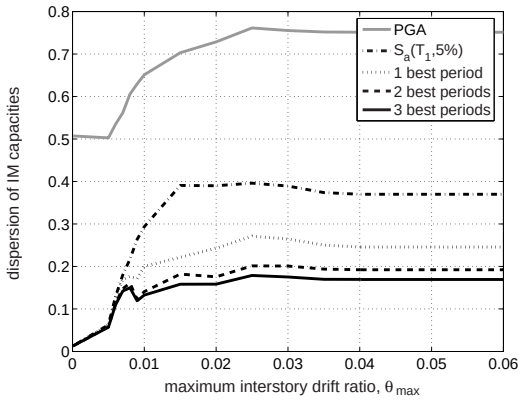

Figure 26. The dispersions for the 5-story building for PGA and $S_a(T_1, 5\%)$ versus the optimal one, two and three periods scalar *IM*s.

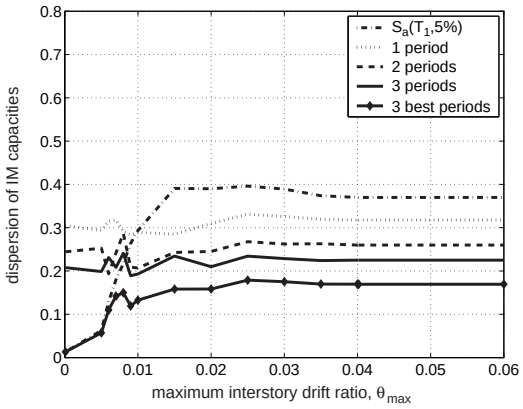

Figure 27. The 84% fractile of the suboptimal dispersion for a single period and power-law forms of two or three periods for the 5-story building, shown versus the dispersion achieved by $S_a(T_1, 5\%)$ and the optimal three-periods power-law *IM*.

In the case of the 9-story building the two optimal periods appear in Figure 28 and the three best in Figure 29. In the first case, the smaller period seems to stay at T_2 while the higher one starts from T_1 and increases to some higher value, only to return back to T_1 again. For the three periods, the results seem to favor one period at T_1, another at T_2 and a third at about twice T_1. Similarly to the 5-story, equal weighting is the optimal strategy for both *IM*s and almost all limit-states. With either two or three periods, as seen in Figure 30, the dispersion reduction is about the same. Actually, the dispersion drops from 40% for one optimal period (or even for just $S_a(T_1, 5\%)$), to less than 25–30% when two or more periods are used. Again, it seems that two spectral values are enough for this first-mode-dominated building and clearly better than just one.

What is of more value though is that the efficiency of the two or three-element *IM* is very stable relative to the choices of the periods and the β, γ weights. In Figure 31 we plot the results of the

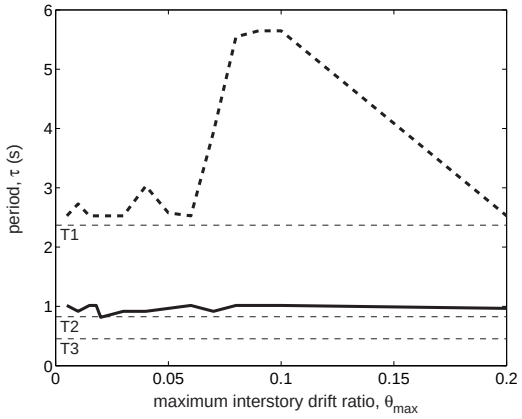

Figure 28. The two optimal periods τ_a, τ_b as they evolve with $\theta_{\max}$ for the 9-story building.

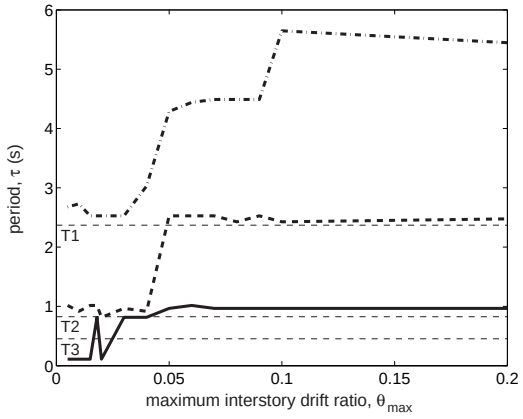

Figure 29. The three optimal periods τ_a, τ_b, τ_c as they evolve with $\theta_{\max}$ for the 9-story building.

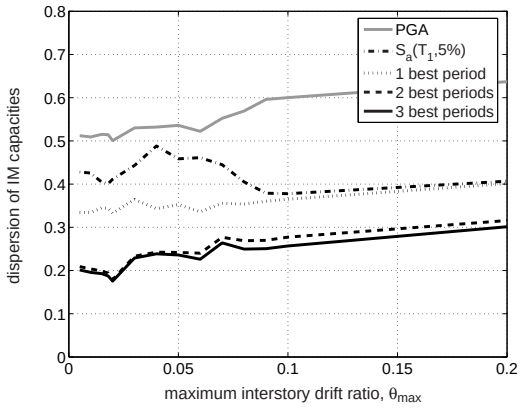

Figure 30. The dispersions for the 9-story building for PGA and $S_a(T_1,5\%)$ versus the optimal one, two and three periods scalar *IM*s.

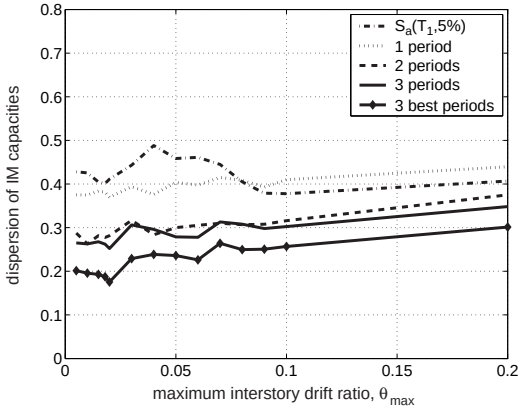

Figure 31. The 84% fractile of the suboptimal dispersion for a single period and power-law forms of two or three periods for the 9-story building, shown versus the dispersion achieved by $S_a(T_1,5\%)$ and the optimal three-periods power-law *IM*.

previously described sensitivity analysis for the 9-story. Clearly, using only one (suboptimal) period is often worse or at most as good as when using $S_a(T_1,5\%)$, as observed in Figure 7 as well. On the other hand, with two or three periods, equally weighted in a power-law form, the *IM* is considerably more robust and relatively reasonable efficiency is maintained. If we follow our observations and set one value around T_1, another at about T_2 and maybe a third 50% or 100% higher than T_1, then weigh them equally ($\beta = 1/2$ or $\beta = \gamma = 1/3$), a dispersion of about 30% is easily achieved in contrast to the elusive single optimal period.

Figure 32 shows the best two periods for the 20-story building. One seems to stay somewhere in the middle of T_2 and T_3 while the other is a lengthened version of the first mode, perhaps by 30–50%. The picture is clearer for the three best periods in Figure 33, where each seems to be a (roughly) 50% lengthened version of one of the three elastic modes, T_1, T_2 and T_3. The optimal weights are roughly

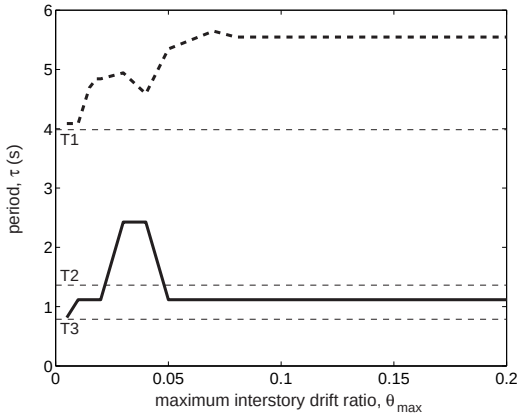

Figure 32. The two optimal periods τ_a, τ_b as they evolve with $\theta_{\max}$ for the 20-story building.

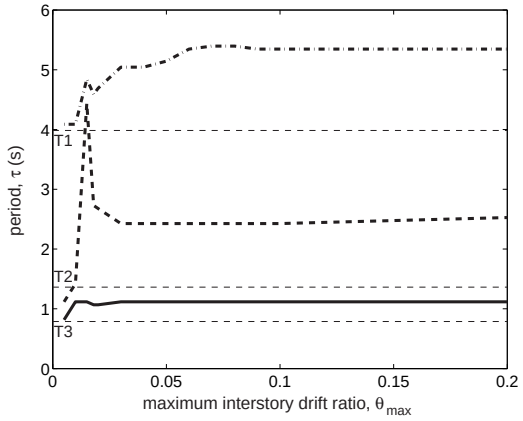

Figure 33. The three optimal periods τ_a, τ_b, τ_c as they evolve with $\theta_{\max}$ for the 20-story building.

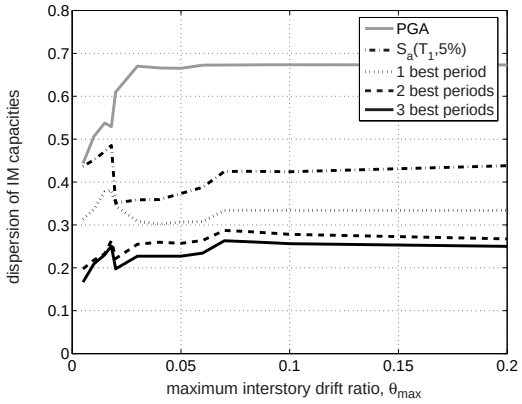

Figure 34. The dispersions for the 20-story building for PGA and $S_a(T_1,5\%)$ versus the optimal one, two and three periods scalar *IM*s.

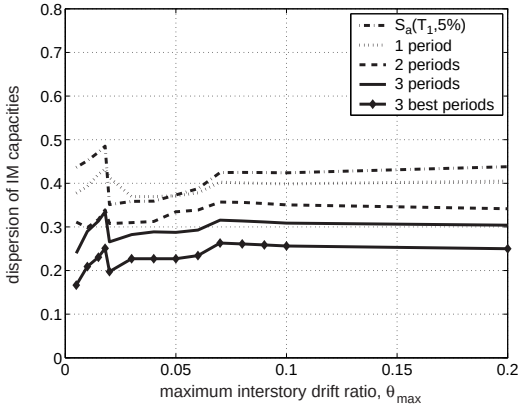

Figure 35. The 84% fractile of the suboptimal dispersion for a single period and power-law forms of two or three periods for the 20-story building, shown versus the dispersion achieved by $S_a(T_1,5\%)$ and the optimal three-periods power-law *IM*.

equal for all two or three periods. The dispersion reduction is significant in both cases, reaching down to 25% versus the 35% achieved by a single optimal period or the 40% of $S_a(T_1,5\%)$ (Figure 34). While the use of three periods rather than two seems to offer little benefit, actually it makes the *IM* quite easier to define. Additionally the results of the sensitivity analysis in Figure 35 suggest that efficiency remains relatively high when three suboptimal periods are employed, versus two or one. Simply by increasing all three elastic periods by some reasonable percentage and employing equal weights ($\beta = \gamma = 1/3$) works fine for all limit-states, achieving dispersions in the order of 30%.

In conclusion, it seems that the use of the power-law form with two or three spectral values helps even when the higher modes are significant. Actually, the more significant they are, the more periods we might want to include. The benefit is not so much in the reduction of dispersion, rather in the robustness of the *IM* and the ability to identify it *a priori*. The sensitivity of the power law *IM*s to suboptimal

user choices significantly decreases when more spectral values are included. Thus, it is not necessary to propose a "magic set" of parameters for each structure: In the inelastic range any reasonably chosen number of equally weighted periods that lie somewhat higher than the elastic ones will provide good dispersion reduction for most cases. Further investigation of more structures is needed before some concrete proposals are made, but the concept looks promising.

6. USING ALL SPECTRAL VALUES

The problems encountered with all previous attempts to use the spectral shape mainly stem from the fact that we were looking for distinct "perfect" periods. This in part made the problem quite more difficult, as we were trying to describe the full spectral shape with only one or two spectral ratios. Using more spectral shape information will hopefully open up some easier paths. Still, visualizing an *IM* vector with more than one spectral ratio would be hard and it would be equally difficult to create enough data to fill the extra dimensions. On the other hand, the collapsed power-law form of the vector to a scalar suggests an easier way to approach this problem. Including more spectral coordinates in Equation (1) is relatively straightforward, while finding the right weight coefficients may be handled by standard linear regression methods, penalized to reflect the sample size limitations.

Taking one step further, there exist methods in statistics that can treat each record's spectrum as a single, functional predictor, thus taking into consideration the shape of the full spectrum and use it as a predictor for limit-state capacity. In formal terms we are proposing the use of a functional linear model (Ramsay and Silverman [15]) that will use each record's spectrum to predict a scalar response, i.e., its limit-state $S_a^{c,i}(T_1,5\%)$-capacity derived from the IDA curve of that i-th record. In essence, we are proposing the use of the linear functional model

$$\ln S_a^{c,i}(T_1,5\%) = \alpha + \int_{t_s}^{t_e} \beta(\tau) \ln\left[\frac{S_a(\tau,5\%)}{S_a(T_1,5\%)}\right] \mathrm{d}\tau + \varepsilon_i \tag{5}$$

where α is the regression intercept, $\beta(\tau)$ is the regression coefficient function, t_s and t_e are the starting and ending periods that bound the spectral region of interest and, finally, ε_i are the independent and normally distributed errors (with a mean of zero).

This can be thought as a conventional multivariate linear regression model, only we can have an infinite number of predictors, or degrees of freedom, in our fitting. Of course, having infinite parameters and only a finite number of responses allows such a model to actually interpolate the responses, if we choose so. This would not provide a meaningful estimator, but can be remedied by sufficiently smoothing the coefficient function $\beta(\tau)$ at a level easily found through cross-validation. We end up with a model to predict limit-state capacities that can be easily imagined to be of the same power-law form as the one we have introduced to collapse the vector of two *IM*s into a scalar in Equation (1). If we use a trapezoidal rule to perform the integration, then we can write Equation (5) as:

$$\begin{aligned}
\ln S_a^{c,i}(T_1,5\%) &\approx \alpha + \sum_{j=1}^{n} \beta(\tau_i) \ln\left[\frac{S_a(\tau_i,5\%)}{S_a(T_1,5\%)}\right] \Delta\tau \quad &\Leftrightarrow \\
S_a^{c,i}(T_1,5\%) &\approx \mathrm{e}^{\alpha} \prod_{j=1}^{n} \left[\frac{S_a(\tau_i,5\%)}{S_a(T_1,5\%)}\right]^{\beta(\tau_i)\Delta\tau} \quad &\Leftrightarrow \\
\mathrm{e}^{\alpha} &\approx S_a^{c,i}(T_1,5\%) \prod_{j=1}^{n} \left[\frac{S_a(\tau_i,5\%)}{S_a(T_1,5\%)}\right]^{-\beta(\tau_i)\Delta\tau} \quad &(6)
\end{aligned}$$

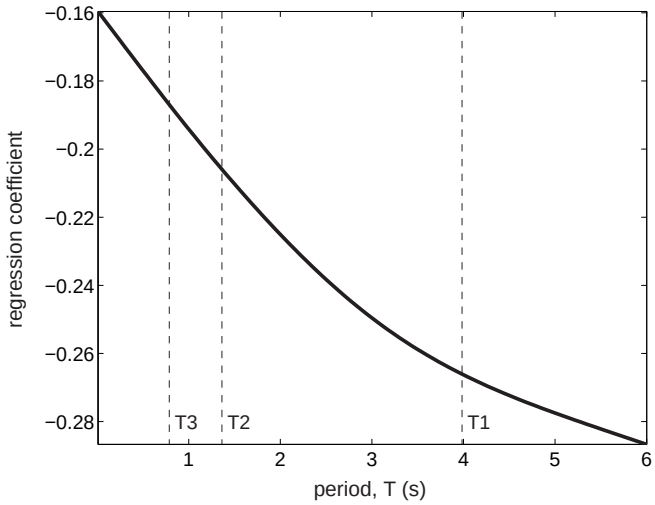

Figure 36. The regression coefficient function $\beta(\tau)$ at global dynamic instability for the 20-story building.

Equation (6) allows us to define a new *IM*, of similar form to Equation (2), that now uses practically the whole spectrum to explain (and reduce) the record-to-record variability. Similarly to the two-periods power-law form, as described in Cordova *et al.* [9], it is expected that hazard curves can be easily determined for such an *IM* without the need for new attenuation relationships.

But why expand to such a complicated *IM*? We have performed such a functional linear fit for the global instability capacities of the 20-story building, using as predictors the spectral coordinates within $t_s = 0.1$s and $t_e = 6$s, and have plotted the coefficient function $\beta(\tau)$ in Figure 36; it precisely explains the influence of every spectral coordinate on the flatline capacity. We can think of $\beta(\tau)$ as a weight function, where its absolute value at each period provides us with the degree of the period's significance to capacity. The importance of spectral coordinates is highest for periods longer than the first mode (high $|\beta(\tau)|$-values), while it decreases rapidly for periods lower than the second mode (low $|\beta(\tau)|$-values). The simplicity of the shape suggests that we can probably provide some general *a priori* suggestions for the coefficient function that will provide relatively efficient *IM*s. Note, that we need not match the actual values of the coefficient function, only its shape, as we are not interested in capacity-prediction, only in capacity dispersion reduction.

Again, the realized gains may not lie as much with dispersion reduction as with robustness. The *IM* suggested by the fit reduces all capacity dispersions for all limit-states by approximately 50% relative to $S_a(T_1, 5\%)$, almost to similar amounts as the power-law form with three periods. Only further investigations can prove whether this functional model will prove more useful or robust than the simpler power-law form. Still, it may help us identify spectral regions of interest and characterize structures in a very simple way.

7. CONCLUSIONS

Providing more efficient Intensity Measures (*IM*s) is a useful exercise, both in reducing the number of records needed for PBEE calculations but also in improving our understanding of the seismic behavior of structures. The record-to-record dispersion in the limit-state *IM*-capacities that is observed with traditional *IM*s can be practically halved by taking advantage of elastic spectrum information. Several methods exist to incorporate elastic spectral values in *IM*s. One could use a single optimally selected spectral value, a vector of two or a power-law combination of several spectral values. While the candidates often seem to achieve similar degrees of efficiency, not all of them are suitable for use *a priori*; it may be quite difficult to select the appropriate periods (or spectral values) before we complete our dynamic analyses. Using a single optimal spectral value is practical only for buildings with insignificant higher modes; taking the spectral value at period higher than the first-mode period provides us with good efficiency even close to global collapse. On the other hand, when the influence of higher modes is significant, a single spectral value is not enough and spectral *shape* becomes important. Then, using two or even three spectral values seems to help both the efficiency and the robustness of the *IM* against the suboptimal selection of periods. A novel method has also been presented that can take advantage of the whole spectrum to provide us with efficient and potentially very robust *IM*s. Additionally, the use of vector *IM*s not only decreases dispersion but it results in summarized IDA *surfaces* that provide a direct visualization of the spectral shape's influence on the capacities for any limit-state. Still, before such *IM*s are adopted significant work remains to be done; we need to investigate more structures and more ground motion records, probably ones with important local spectral features, e.g., soft soil or directivity influence. Thus we will be able to better select the appropriate *IM* that will be both efficient and sufficient for a given structure and site.

ACKNOWLEDGEMENT

Financial support for this research was provided by the sponsors of the Reliability of Marine Structures Affiliates Program of Stanford University.

REFERENCES

1. Vamvatsikos D, Cornell CA. Incremental dynamic analysis. *Earthquake Engineering and Structural Dynamics* 2002; **31**(3):491–514.
2. FEMA. Recommended seismic design criteria for new steel moment-frame buildings. *Report No. FEMA-350*, SAC Joint Venture, Federal Emergency Management Agency, Washington DC, 2000.
3. Vamvatsikos D, Cornell CA. Applied incremental dynamic analysis. *Earthquake Spectra* 2004; **20**(2):523–553.
4. Vamvatsikos D, Cornell CA. Direct estimation of the seismic demand and capacity of oscillators with multi-linear static pushovers through incremental dynamic analysis. *Earthquake Engineering and Structural Dynamics* 2005; In review.
5. Luco N. Probabilistic seismic demand analysis, SMRF connection fractures, and near-source effects. PhD Dissertation, Department of Civil and Environmental Engineering, Stanford University, Stanford, CA, 2002. http://www.stanford.edu/group/rms/Thesis/Luco_Dissertation.zip [Feb 12th, 2005].
6. Shome N, Cornell CA. Probabilistic seismic demand analysis of nonlinear structures. *Report No. RMS-35*, RMS Program, Stanford University, Stanford, CA, 1999. http://www.stanford.edu/group/rms/Thesis/NileshShome.pdf [Feb 12th, 2005].
7. Carballo JE, Cornell CA. Probabilistic seismic demand analysis: Spectrum matching and design. *Report No. RMS-41*, RMS Program, Stanford University, Stanford, CA, 2000. http://www.stanford.edu/group/rms/Reports/RMS41.pdf [Feb 12th, 2005].
8. Mehanny SS, Deierlein GG. Modeling and assessment of seismic performance of composite frames with reinforced

concrete columns and steel beams. *Report No. 136*, The John A.Blume Earthquake Engineering Center, Stanford University, Stanford, CA, 2000.
9. Cordova PP, Deierlein GG, Mehanny SS, Cornell CA. Development of a two-parameter seismic intensity measure and probabilistic assessment procedure. In *Proceedings of the 2nd U.S.-Japan Workshop on Performance-Based Earthquake Engineering Methodology for Reinforced Concrete Building Structures*. Sapporo, Hokkaido, 2000; 187–206.
10. Bazzurro P, Cornell CA. Seismic hazard analysis for non-linear structures. II: Applications. *ASCE Journal of Structural Engineering* 1994; **120**(11):3345–3365.
11. Lee K, Foutch DA. Performance evaluation of new steel frame buildings for seismic loads. *Earthquake Engineering and Structural Dynamics* 2002; **31**(3):653–670.
12. Luco N, Cornell CA. Effects of connection fractures on SMRF seismic drift demands. *ASCE Journal of Structural Engineering* 2000; **126**:127–136.
13. Hastie TJ, Tibshirani RJ. *Generalized Additive Models*. Chapman & Hall: New York, 1990.
14. Efron B, Tibshirani RJ. *An Introduction to the Bootstrap*. Chapman & Hall/CRC: New York, 1993.
15. Ramsay JO, Silverman BW. *Functional Data Analysis*. Springer: New York, 1996.

